1 Anhydrite Dissolution Dynamics as a Hydrogeochemical

Tracer of Seismic-Fluid Coupling: Insights from the East

3 Anatolian Fault Zone, Turkey

- 4 Zebin Luo¹, Xiaocheng Zhou^{2,3}, Yueren Xu², Peng Liang², Huiping Zhang⁴, Jinlong
- 5 Liang⁵, Zhaojun Zeng², Yucong Yan³, Zheng Gong⁶, Shiguang Wang⁶, Chuanyou Li⁴,
- 6 Zhikun Ren⁴, Jingxing Yu⁴, Zifa Ma⁴, Junjie Li⁴
- 7 ¹School of Emergency Management, Xihua University, Chengdu 610039, China
- 8 ²United Laboratory of High-Pressure Physics and Earthquake Science, institute of earthquake forecasting,
- 9 CEA, Beijing 100036, China
- ³School of Earth Sciences and Resources, China University of Geosciences, Beijing 100083, China
- ⁴Institute of Geology, China Earthquake Administration, Beijing, 100081, China
- ⁵College of Earth and Planetary Sciences, Chengdu University of Technology, Chengdu 610059, China
- 13 ⁶ Institute of Geophysics, China Earthquake Administration, Beijing, 100081, China
- 14 Correspondence to: Xiaocheng Zhou (<u>zhouxiaocheng188@163.com</u>).

15 Abstract: Pre-seismic turbidity and salinity anomalies in groundwater were documented at HS04 and 16 HS14 monitoring wells and/or springs along the East Anatolian Fault Zone (EAFZ) following the 2023 Mw 7.8 and Mw 7.6 Turkey earthquakes. By synthesizing hydrogeochemical datasets (2013-2023) with 17 18 post-seismic responses, we unravel fault-segmented groundwater evolution: (1) Northern Na-Cl and Na-19 HCO₃ type waters result from mixing of mantle-derived magmatic fluids (0-7% contribution) with shallow groundwater, governed by volcanic rocks-carbonate dissolution; (2) Central-southern Ca-HCO₃ 20 and Ca-Na-HCO3 systems reflect shallow circulation with localized inputs from evaporites (Increased 21 SO₄²⁻ concentration caused by dissolution of anhydrite), ophiolites (Mg²⁺ anomalies), and seawater. 22 PHREEQC simulation shows that the dissolve-precipitation equilibrium of anhydrite is sensitive to the 23 24 variation of water-rock reaction intensity in the Central-southern segments of EAFZ. Coseismic 25 permeability changes disrupt the solubility equilibria of anhydrite, driving hydrochemical anomalies. We 26 propose that seismic stress redistribution induces fracture network reorganization, thereby disrupting 27 anhydrite solubility equilibria. Given its tectonic sensitivity and widespread occurrence, anhydrite 28 dissolution dynamics emerge as a potential tracer for hydrogeochemical monitoring in active fault zones. 29 We propose a novel research paradigm wherein regional hydrogeological surveys identify applicable 30 target indicator horizons, enabling continuous monitoring and establishment of region-specific 31 evaluation metrics to ultimately achieve early warning capabilities for geohazard precursors.

- Key words: Groundwater; Water-rock interaction; Seismic activity; PHREEQC; Anhydrite; East
- 33 Anatolian Fault Zone.

32

34

35

36

37

38

39

40

41

42

43

44

45

46

47

48

49

50

51

52

53

54

55

56

57

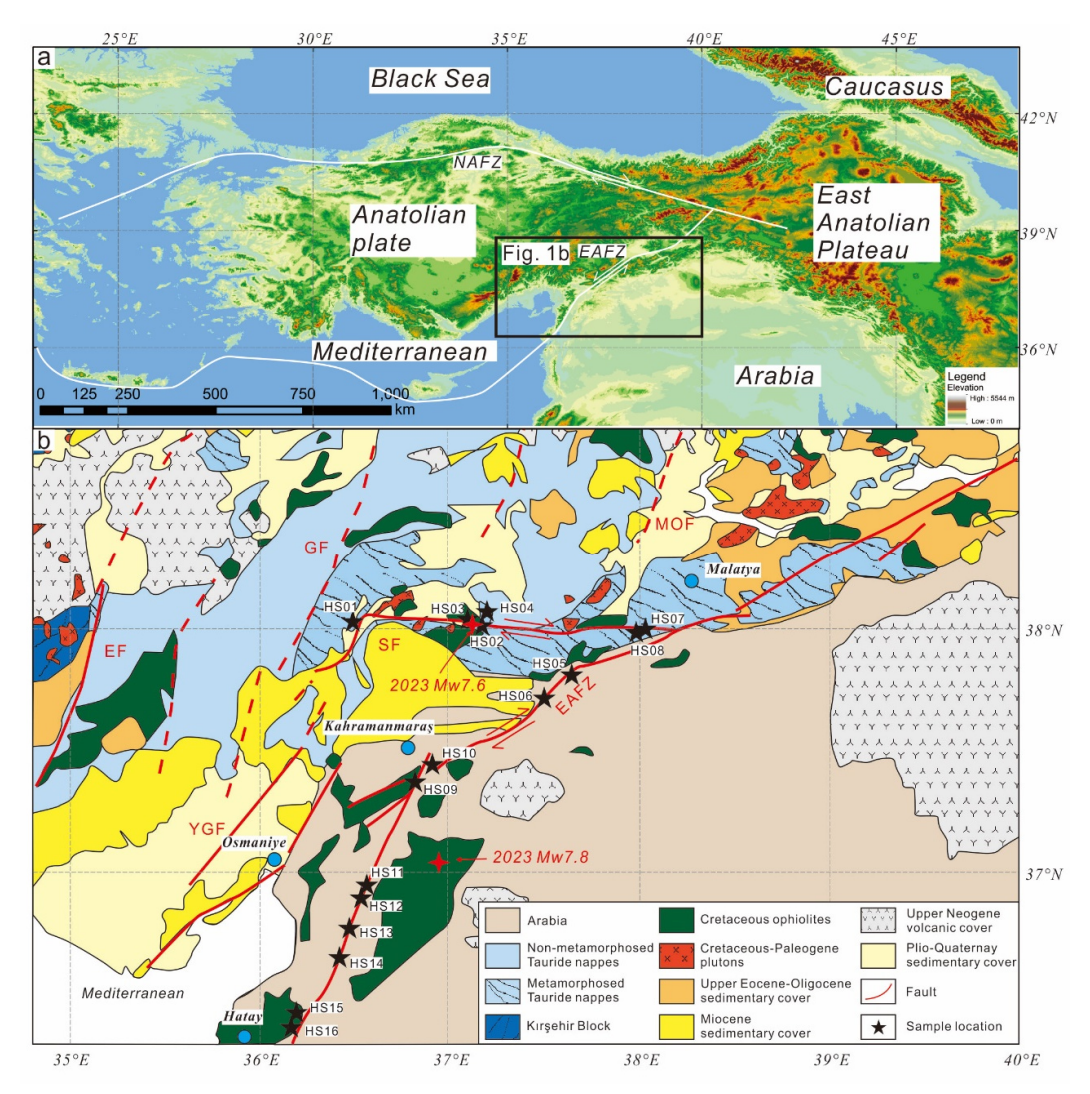
58

59

1 Introduction

Active fault zones perturb subsurface hydrogeochemical equilibrium through dynamic rock-water interactions, generating diagnostic anomalies in groundwater chemistry that may serve as potential seismic precursors (Franchini et al., 2021; Ingebritsen and Manga, 2014; King et al., 2006; Luo et al., 2023; Poitrasson et al., 1999; Skelton et al., 2014; Tsunogai and Wakita, 1995; Wang et al., 2021). However, the diagnostic reliability of such hydrochemical signatures faces challenges. Climatic factors (e.g., precipitation variability and temperature fluctuations) can mask tectonic signals by altering waterrock reaction kinetics (Okan et al., 2018), while regional heterogeneity in lithology, fracture density, and hydrological circulation depth introduces substantial spatial variability in groundwater (Luo et al., 2023). This study investigates the hydrogeochemical characteristics of the seismically active East Anatolian Fault Zone (EAFZ) in eastern Turkey through a comprehensive 13-year observational dataset (2013-2023). By systematically analyzing groundwater circulation patterns and water-rock interaction processes along the fault system, we integrate post-seismic hydrochemical monitoring following the February 2023 Mw 7.8 and 7.6 earthquake sequence to delineate the relationship between hydrogeochemical anomalies and fault activity. Our findings aim to establish the relationship between groundwater anomalies and fault zone activities, thereby advancing methodologies for groundwaterbased seismic monitoring in active fault zone systems. The EAFZ, a ~500 km NE-SW trending left-lateral strike-slip system accommodating ~11 mm/yr of Anatolian-Arabian plate motion with reverse thrust components (Pousse - Beltran et al., 2020), has generated destructive seismic events throughout recorded history (Hubert-Ferrari et al., 2020; Simão et al., 2016; Sparacino et al., 2022; Tan et al., 2008). The 2023 twin earthquakes exemplify its capacity for massive stress release (Kwiatek et al., 2023; Ma et al., 2024; Wang et al., 2023b), producing coseismic surface ruptures exceeding 280 km with maximum slip of 7.2±0.72 m (Liang et al., 2024). Notably, marked hydrochemical anomalies (e.g., white water, turbidity and intermittent groundwater gushing) were detected at monitoring spring HS04 and well HS14 both before and after the earthquake (Video 1 and 2), indicating fault-controlled fluid responses to seismic stress perturbations.

Previous studies have identified three primary fluid sources within the EAFZ system: 1) mantle-derived magmatic fluids (Aydin et al., 2020; Italiano et al., 2013; Karaoğlu et al., 2019), 2) deeply circulated metamorphic waters (Yuce et al., 2014), and 3) Mediterranean seawater intrusion at its southern terminus (Yuce et al., 2014). These studies provide sufficient data support for accurate understanding of EAFZ groundwater circulation. In this contribution, the EAFZ groundwater observation data over the past 13 years are compared with the groundwater chemical composition after the double earthquakes in 2023 to tracing the origin of groundwater, restore the water-rock interaction process, and evaluate the influence of seismic activity on the groundwater circulation process. We have proposed that an abnormality in groundwater chemical components, which does not require the involvement of deep fluids, could potentially serve as a basis for earthquake prediction. It provides new constraints on tectonic controls of deep fluid migration in active fault zone systems while advancing the application of hydrogeochemical monitoring in seismic hazard assessment.



- 73 Fig. 1. a: A brief Map of the eastern Mediterranean region from NASADEM
- 74 (https://doi.org/10.5069/G93T9FD9). b: Geological map of EAFZ, modified from (van Hinsbergen et al.,
- 75 2024). EF: Ecemiş Fault, SF: Sürgü Fault, MOF: Malatya-Ovacık Fault, GF: Göksün Fault, YGF: Yeşilgöz-
- 76 Göksün Fault.

77

2 Geologic background

78 Located at the intersection of Eurasia, Africa and Arabia, Turkey has a complex tectonic background 79 (Lanari et al., 2023; Simão et al., 2016). Here, the collision between the Arabian and Eurasian plates was 80 an important tectonic process that began in the early Miocene (~ 23 Ma) and continues to the this day 81 (van Hinsbergen et al., 2024). This collision caused plateau uplift, volcanic eruptions, sedimentary basin 82 formation, and large-scale strike-slip faults in eastern Turkey, including the EAFZ (Fig. 1) (Bilim et al., 83 2018; Karaoğlu et al., 2018; Karaoğlu et al., 2020; Whitney et al., 2023; Yönlü et al., 2017; Zhou et al., 84 2024). 85 The formation of the EAFZ is related to the northward subduction of a strong and thin lithospheric wedge under the Arabian Plate (Nalbant et al., 2002; Sparacino et al., 2022). This subduction process led to the 86 87 formation of a stress concentration zone that eventually developed into a strike-slip fault that penetrated 88 the entire lithosphere, i.e. the EAFZ (Nalbant et al., 2002). In addition, because the African plate and the 89 Arabian plate are still moving northward, this fault zone is also accompanied by a certain thrust process, 90 which causes huge stresses at the plate margin (Ma et al., 2024; Över et al., 2023; Özkan et al., 2023; 91 Pousse - Beltran et al., 2020; Wang et al., 2023b; Whitney et al., 2023). The stratigraphic composition of the East Anatolian fault zone is complex, including Non-92 93 metamorphosed Tauride nappes and Metamorphosed Tauride nappes crystallization base, Cretaceous 94 ophiolites and Cretaceous-Paleogene plutons. It is overlaid by clastic deposits, lacustrine deposits (such 95 as: Ancient Amik Lake) and volcanic cover of Upper Eocene-Oligocene to Plio-Quaternay. Faults are 96 widely developed in study area, including East Anatolian Fault, Ecemiş Fault, Sürgü Fault, Malatya-97 Ovacık Fault, Göksün Fault, Yesilgöz-Göksün Fault etc. (van Hinsbergen et al., 2024). These faults has 98 been active for a long time and has a history of devastating earthquakes, including two in February 2023 99 (Mw 7.8 and Mw 7.6) (Fig. 1) (Carena et al., 2023; Kwiatek et al., 2023; Ma et al., 2024; Maden and Özt 100 ürk, 2015; Över et al., 2023; Özkan et al., 2023; Pousse - Beltran et al., 2020; Tan et al., 2008; Wang et 101 al., 2023b).

The climate of the EAFZ is mainly a temperate continental climate with cold winters and hot and dry summers. The average annual rainfall is between 200 mm and 600 mm, and is mainly winter rain. Due to its inland location and low rainfall, the flow of the river is relatively small. The groundwater system is relatively complex, and geothermal resources are mainly distributed near the fault zone and its controlled areas, including low or moderate temperature geothermal systems, which have great potential for development and utilization (Aydin et al., 2020; Güleç and Hilton, 2016; Inguaggiato et al., 2016; Karaoğlu et al., 2019).

3 Sampling and analytical methods

102

103

104

105

106

107

108

109

110

111

112

113

114

115

116

117

118

119

120

121

122

123

124

125

126

127

128

129

16 samples of groundwater were collected in EAFZ, including hot springs, geothermal wells and river water. HS01-HS04 was collected from west to east along SF. HS07-HS16 was collected from north to south along EAFZ (Fig. 1). Detailed sample collection and testing methods can be found at Luo et al. (2023). In short, the water sample was taken with a 50 mL clean polyethylene bottle and the temperature and pH of the water were measured and recorded. Two samples were collected at each sampling site, one was added with ultrapure HNO₃ to analyse the cation content, and the other was used to analyse the anion content and isotopic composition. All samples need to be pre-treated with a 0.45 µm filter membrane to remove impurities before sampling. The Hydrogen and oxygen isotopes were determined by a Picarro L2140-I Liquid water and vapor isotope analyzer (relative to Vienna Standard Mean Ocean Water (V - SMOW)). Precisions on the measured δ^{18} O and δD value was $\pm 0.2\%$ (2SD) and $\pm 1\%$ (2SD) respectively (Zeng et al., 2025). The cation (Li⁺, Na⁺, K⁺, Ca²⁺ and Mg²⁺) and anion (F⁻, Cl⁻, NO₃⁻ and SO₄²⁻) were analysed by Dionex ICS-900 ion chromatograph (Thermo Fisher Scientific Inc.) at the Earthquake Forecasting Key Laboratory of China Earthquake Administration, with the reproducibility within ±2% and detection limits 0.01 mg/L (Chen et al., 2015). HCO₃⁻ and CO₃²⁻ was determined by acid-base titration with a ZDJ-100 potentiometric titrator (reproducibility within ±2%). SiO₂ were analysed by inductively coupled plasma emission spectrometer Optima-5300 DV (PerkinElmer Inc.) (Li et al. 2021). Trace elements were analysed by Element XR ICP-MS at the Test Center of the Research Institute of Uranium Geology. Multielement standard solutions (IV-ICPMS 71A, IV-ICP-MS 71B and IV-ICP-MS 71D, iNORGANIC VENTURES) used for quality control. The analytical error margin of major cations and trace elements

were less than 10%. Strontium isotope ratios (87 Sr/ 86 Sr) were determined through triple quadrupole ICP-MS (Agilent 8900 ICP-QQQ) with a precision of ± 0.001 (Liu et al., 2020).

4 Results

Physical, chemical and isotopic compositions of groundwaters are listed in Table 1. The variation range of EC is 275 - 2683 µs/cm. The pH of the water samples varied from 7.03 to 11.72, and all the samples showed weakly alkaline characteristics except HS15 (pH=11.72). The effluent temperature of water sample is low (8.1–32.0°C), and the highest temperature is HS15 sample (32.0°C). HS08 is a river sample with the lowest temperature (8.1°C). The differences in temperature between the samples reflect specific hydrological processes. SiO₂ varies from 0.38 mg/L to 84.64mg/L. HCO₃⁻ (165.72–1854.30 mg/L) is the main anion. The concentration of SO₄²⁻ range from 1.21 mg/L to 316.61 mg/L, and the concentration of SO₄²⁻ in some samples is relatively high (e.g. HS01 (287.74 mg/L), HS03 (103.56 mg/L), HS04 (229.75 mg/L), HS14 (316.61 mg/L)). The concentration of Na⁺ (0.42–88.93 mg/L), Cl⁻ (0.97–75.92 mg/L) and B (3.62–1047.25 µg/L) varied synergistically. Ca²⁺ (14.16–501.58 mg/L) is the main cation, followed by Mg²⁺ (0.38–116.20 mg/L). The types of groundwater include Na-Cl-HCO₃, Ca-HCO₃, Ca-HCO₃-SO₄ and Mg-HCO₃ (Fig. 2 and Fig.S1). The δ ¹⁸O and δ D of samples varied from –11.30% to –6.55% and –65.43% to –34.43% respectively, which is near to the global meteoric water line (GMWL) (Craig, 1961) (Fig. 3), suggesting their meteoric water origin. The ⁸⁷Sr/⁸⁶Sr varied from 0.7053 to 0.7135, showing the characteristics of multi-source region mixing.

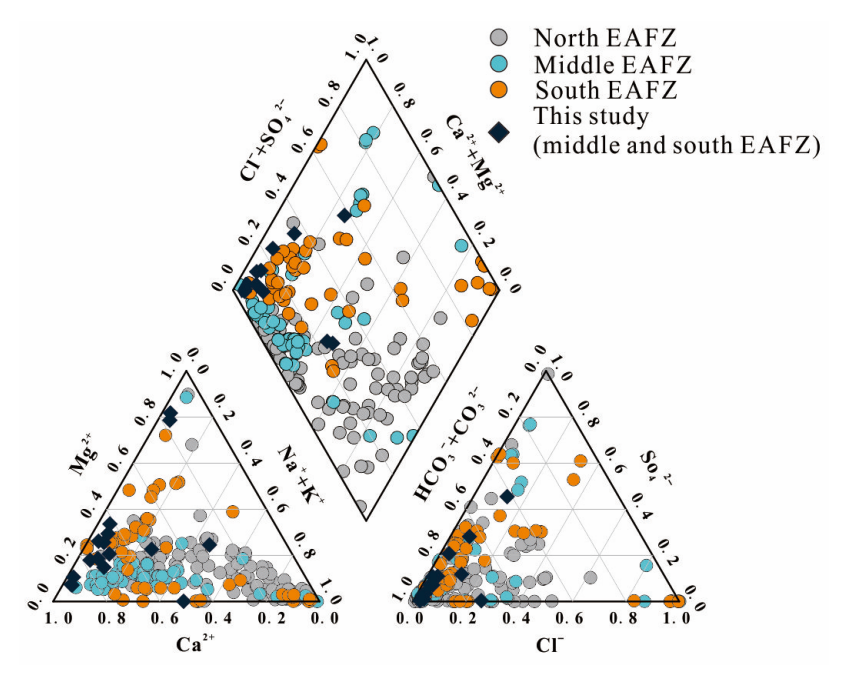


Fig. 2. Piper plot of sampled groundwaters in EAFZ. The groundwaters are Na-Cl-HCO₃, Ca-HCO₃, Ca-HCO₃-SO₄ and Mg-HCO₃ types. Literature data source (see Table S1 for details): (Aydin et al., 2020; Baba et al., 2019; Karaoğlu et al., 2019; Okan et al., 2018; Pasvanoglu, 2020; YASİN and YÜCE, 2023; Yuce et al., 2014)

The composition of trace elements in groundwaters are shown in Table 2. The contents of Sr (30.13–3244.88 μ g/L) and Ba (1.89–196.48 μ g/L) in the samples varied widely. Moreover, Sr and SO₄^{2–} had obvious positive correlation. Box plot analysis showed that the Fluid-Mobile Element (FME) concentrations of B (3.62–1047.25 μ g/L), Li (0.33–89.93 μ g/L) and Rb (0.14–28.91 μ g/L) in some samples were greater than the median (Fig. S2). Enrichment coefficients (EF) normalized by Ti is used for groundwaters and rocks. The result shows that whether compared with schist, basalt or Andesite of EAFZ, trace elements in groundwaters are all in a state of enrichment, and some elements can even be enriched 100000 times (Fig. S3). The distribution patterns of trace elements in all water samples maintained a good consistency, and no abnormal changes in trace elements in specific areas (such as Pb) were observed (Fig. S3). This indicates that the circulation of regional groundwater is only minimally affected by human activities.

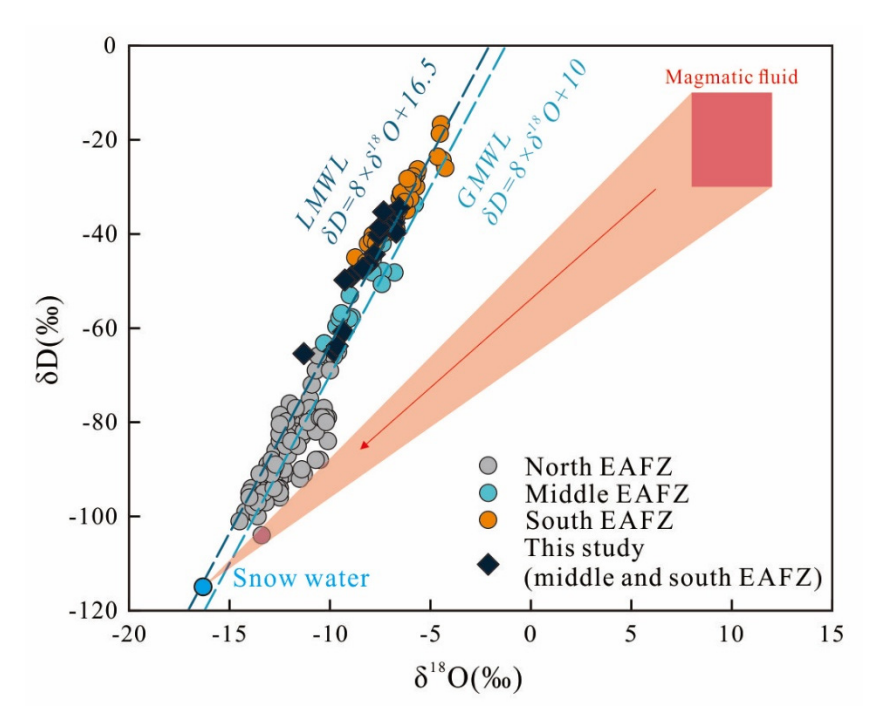


Fig. 3. δD and $\delta^{18}O$ (%V-SMOW) values for groundwaters collected from EAFZ. The GMWL represents the global meteoric water line (Craig, 1961). The LMWL represents the Local meteoric water line (Aydin et al., 2020). The magmatic fluid distribution ($\delta D = -20 \pm 10\%$, $\delta^{18}O = 10 \pm 2\%$) from (Giggenbach, 1992). Snow water ($\delta D = -115\%$, $\delta^{18}O = -16.3\%$) from (Andy et al., 2020) (The sampling elevation is approximately 2000m). Literature data source is consistent with Fig. 2.

Table 1.Physical, Chemistry and isotopic compositions of groundwaters from the EAFZ. 170

Į,	Long(E)	lat (N)	Ę	5	Г	11"	EC	$S1O_2$	L_1^{τ}	Na	\mathbf{K}^{+}	${ m Mg}^{z_{ m T}}$	Ca^{2+}	F.	Cŀ	NO_3 -	SO_4^{2}	HCO_3	CO_{3}^{2}	δD	$\delta^{18}O$	875/865	תיינ
•	(°)	(°)	1 ype	Date	(oC)) ud	(μS/cm) ((mg/L)	(mg/L)	(mg/L)	(mg/L)	(mg/L)	(mg/L)	(mg/L)	(mg/L)	(mg/L)	(mg/L)	(mg/L)	(mg/L)	(%)	(%0)	SI/ SI	2SD
HS01	36.518113	38.003517	S	03/23/2023	15.8	8.12	1565	20.70	1	27.93	4.85	75.69	253.85	3.60	55.46	Î	287.74	670.01	1	-64.93	-9.81	0.7065	0.0001
HS02	37.173212	38.028567	S	03/23/2023	13.2	8.35	287	5.27	1	0.42	1	6.58	54.04	0.40	1.33	5.06	6.37	178.53	1	-65.43	-11.30	0.7120	0.0003
HS03	37.166040	38.031327	S	03/23/2023	13.2	7.12	1876	26.36	0.13	48.44	0.48	74.20	368.42	0.50	30.85	30.13	103.56	1271.1	•	-60.77	-9.33	0.7079	0.0002
HS04	37.174886	38.033718	S	03/23/2023	15.0	7.03	2683	84.64	0.05	19.90	0.46	116.20	501.58	3.70	9.29	3.33	229.75	1854.3	•	-63.82	-9.64	0.7132	0.0008
HS05	37.669088	37.809271	S	03/23/2023	12.7	8.50	634	14.42	•	99.7	0.39	25.88	103.61	0.53	4.43	12.92	29.75	367.72	1	-44.29	-7.79	0.7091	0.0003
90SH	37.510811	37.700516	S	03/23/2023	15.0	8.27	774	15.34	•	4.19	0.32	54.08	100.99	0.43	5.98	1.61	7.96	515.66	1	-46.53	-8.11	0.7100	0.0002
HS07	38.056844	37.942560	S	03/23/2023	8.6	8.46	276	9.41	•	0.84	•	4.62	55.11	0.41	0.97	2.74	5.00	167.86	1	-49.09	-8.93	0.7135	0.0006
HS08	38.051818	37.939222	~	03/23/2023	8.1	8.43	275	15.15	٠	1.13	٠	4.47	55.34	0.44	1.06	3.83	5.69	165.72	1	-49.81	-9.26	0.7104	0.0004
HS09	36.808379	37.349742	S	03/23/2023	18.0	8.11	669	25.50	0.01	5.85	0.21	42.60	94.99	0.52	6.80	8.87	93.44	344.96	1	-37.65	-6.81	0.7076	0.0002
HS10	36.994384	37.460028	S	03/23/2023	20.0	8.48	659	31.29	•	1.57	•	90.13	18.22	0.35	3.80	7.53	2.76	459.47	1	-39.65	-6.71	0.7119	0.0003
HS11	36.554302	36.892454	S	03/23/2023	16.3	8.27	517	69.6	٠	2.32	0.09	27.89	75.25	0.45	4.39	9.25	12.11	312.24	1	-40.30	-7.58	0.7107	0.0004
HS12	36.521328	36.811041	S	03/23/2023	16.9	8.32	489	46.50	٠	2.11	•	92.09	14.16	0.52	6.13	14.55	4.27	307.98	1	-34.43	-6.55	0.7110	0.0006
HS13	36.439440	36.672020	S	03/23/2023	18.2	8.22	579	10.05	0.01	4.87	0.49	30.35	81.56	0.50	7.67	8.67	39.89	309.40	1	-37.88	-7.30	0.7080	0.0002
HS14	36.373823	36.503634	W	03/23/2023	23.5	8.21	1305	36.64	0.09	62.40	5.79	65.12	151.43	4.33	75.92	34.60	316.61	300.15	1	-38.61	-7.51	0.7053	0.0001
HS15	36.163672	36.383335	S	03/23/2023	32.0	11.72	589	0.38	0.02	48.64	1.42	0.38	55.55	0.41	48.71	5.28	1.21	1	154.61	-47.27	-8.37	0.7070	0.0007
HS16	36.147159	36.273720	S	03/23/2023	24.5	8.45	1100	32.57	0.01	88.93	18.68	59.60	73.35	0.72	67.11	43.51	75.90	484.37	'	-35.34	-7.33	0.7073	0.0002

Note: "-" represents below detection limit or undetected. "S" is Spring, "W" is Well water, "R" is River water.

172 Table 2. Trace elements compositions of groundwaters from the EAFZ.

Note: "-" represents below detection limit or undetected. Hf and Ta are kept to 3 decimal places due to their low content.

5 Discussion

174

175

176

177

178

179

180

181

182

183

184

185

186

187

188

189

190

191

192

193

194

195

196

197

198

199

200

201

5.1 The origin of groundwater in different segments of EAFZ

Previous studies have documented abundant geothermal resources within the EAFZ, which is characterized by low or moderate temperature geothermal systems (Aydin et al., 2020; Baba et al., 2019). Both aqueous and gaseous geochemical signatures indicate mixing between deep-sourced mantle/crustal fluids and shallow groundwater reservoirs (Aydin et al., 2020; Italiano et al., 2013; Yuce et al., 2014). Yuce et al. (2014) proposed that geothermal fluids at the southwest end of the EAFZ are triggered by deep-rooted regional faults, with localized seawater intrusion. Analogously, there are deep components involved in the geothermal fluid circulation in the middle to east section of EAFZ. However, the source of deep components are thought to be controlled by magmatic activity rather than from deep-rooted regional faults (Aydin et al., 2020; Italiano et al., 2013; Karaoğlu et al., 2019). At the intersection of the EAFZ and the North Anatolian Fault Zones (NAFZ), which is also known as the Karliova triple junction, there is extensive volcanic activity that may have provided energy and components for the geothermal fluid cycle eastern segment of the EAFZ (Bilim et al., 2018; Karaoğlu et al., 2018; Karaoğlu et al., 2020). Furthermore, Italiano et al. (2013) suggested these volcanic activities may even contribute to geothermal fluids in the middle segment of the EAFZ. These findings collectively suggest multiple tectonic controls (volcanism, fault activity, and seawater intrusion) on EAFZ's geothermal systems. The February 2023 earthquake sequence (Mw 7.8 and 7.6) ruptured the central EAFZ segment. A critical question arises: Are the observed pre-seismic groundwater anomalies (white water, turbidity and intermittent groundwater gushing) (Video 1 and Video 2) seismogenically linked to this seismic event? To address this, we conducted comparative analyses of post-seismic hydrochemical data against a decadal-scale (13-year) pre-seismic groundwater dataset, as detailed below:

5.1.1 Hydrogen and oxygen isotope characteristics of groundwaters

Hydrogen and oxygen isotopes serve as robust geochemical tracers for elucidating the origin of geothermal fluids groundwater. As illustrated in Fig. 3, the δD and $\delta^{18}O$ compositions of groundwater in the EAFZ align closely with the GMWL (Craig, 1961), indicating predominant atmospheric precipitation recharge. Notably, groundwater in the southern EAFZ proximal to the Mediterranean Sea exhibits progressively heavier isotopic signatures toward the coast, consistent with recharge sourced from

evaporated Mediterranean seawater. In contrast, some northern groundwater displays distinct $\delta^{18}O$ enrichment deviating from local meteoric trends, indicative of mixing with deep-sourced magmatic fluids—a interpretation corroborated by widespread Quaternary volcanic activity in the northern sector (Fig. 3) (Bilim et al., 2018; Karaoğlu et al., 2018; Karaoğlu et al., 2020). Conversely, central and southern groundwater samples exhibit isotopic signatures decoupled from magmatic inputs, reflecting the absence of active deep-seated magma reservoirs in these segments.

The groundwater chemistry exhibits distinct spatial heterogeneity across the EAFZ segments. Northern

5.1.2 Major ion characteristics of groundwaters

202

203

204

205

206

207

208

209

210

211

212

213

214

215

216

217

218

219

220

221

222

223

224

225

226

227

228

229

groundwaters are significantly enriched in Na+, K+, and Cl- (Na-Cl and Na-HCO3 type), whereas central and southern segments display Ca-Mg-HCO3 type waters, with localized Ca-SO4 and Na-Cl anomalies (Fig. 2). These hydrochemical disparities likely reflect fundamentally distinct recharge sources and circulation pathways. As discussed earlier, magmatic fluid contributions are evident in northern groundwaters. Chloride serves as a key tracer for magmatic input (Luo et al., 2023; Pan et al., 2021). In the eastern EAFZ, Clconcentrations span 0.4-2500 mg/L, markedly higher than central/southern values. Given the segment's inland setting, seawater intrusion is negligible, suggesting Cl- enrichment primarily originates from magmatic fluids. Notably, Na⁺/Cl⁻ molar ratios deviate from theoretical mixing trends, with Na⁺ excesses implicating additional sodium sources (e.g., albite dissolution), to be detailed in Section 5.2. This interpretation aligns with petrological and geophysical evidence of active magmatism in the eastern EAFZ (Bilim et al., 2018; Karaoğlu et al., 2018; Karaoğlu et al., 2020; Maden and Öztürk, 2015; Oyan, 2018). Integrated H-O isotopic, major ion, and volcanic activity data collectively support a mixing model between meteoric water and magmatic fluids in the northern EAFZ. In contrast, central and southern groundwaters exhibit lower Na⁺ and Cl⁻ concentrations, with sporadic anomalies attributable to evaporite dissolution or limited seawater influence (Table 1). The Ca-Mg-HCO3 dominance, coupled with isotopic signatures, reflects shallow circulation systems (<5 km depth) devoid of significant deep tectonic/magmatic inputs (Table S2). Ca²⁺ likely derives from calcite, dolomite, or plagioclase weathering, while Mg²⁺ sources include dolomite and serpentinite. Pre-seismic turbidity at HS14 (Video 1) may indicate earthquake-induced disruption of water-rock equilibria.

However, the geothermal gases in the centre and south segment of EAFZ exhibit mantle-like $\delta^{13}C_{CO_2}$ (-5.6% to -0.2%) and elevated ${}^{3}\text{He}/{}^{4}\text{He}$ ratios (Rc/Ra = 0.44–4.41), contrasting with the absence of deep fluid signatures in groundwater (Italiano et al., 2013). Actually, this decoupling results from fundamentally distinct migration mechanisms. Groundwater circulation operates as a shallow crustal system dominated by meteoric recharge, structurally confined by fault architecture. Conversely, geothermal gases predominantly represent deep-seated fluids, with their high mobility and low density enabling efficient ascent through fractures. This explains why mantle/crustal signals are preserved in gases but attenuated in aqueous phases. To further constrain groundwater source area, we have calculated the thermal reservoir temperature of EAFZ groundwater, and the results are shown in Table S2. Due to the low water-rock interaction degree and diversity of rock types in this area, cations in water are difficult to reach water-rock equilibrium (Fig. 4). Hence, most of the cationic thermometer estimates are too large or too small, which can only be used as a reference for thermal reservoirs. Fortunately, SiO₂ thermometers are relatively suitable for estimating the reservoir temperature. As can be seen from Table S2, the reservoir temperatures range from 19.81°C to 128.09 °C (Quartz, no steam loss), which belongs to the low or moderate temperature geothermal systems. Using the circulation depth calculation formula, the maximum circulation depth is estimated to be 4.4km (HS04) (Table S2).

230

231

232

233

234

235

236

237

238

239

240

241

242

243

244

245

246

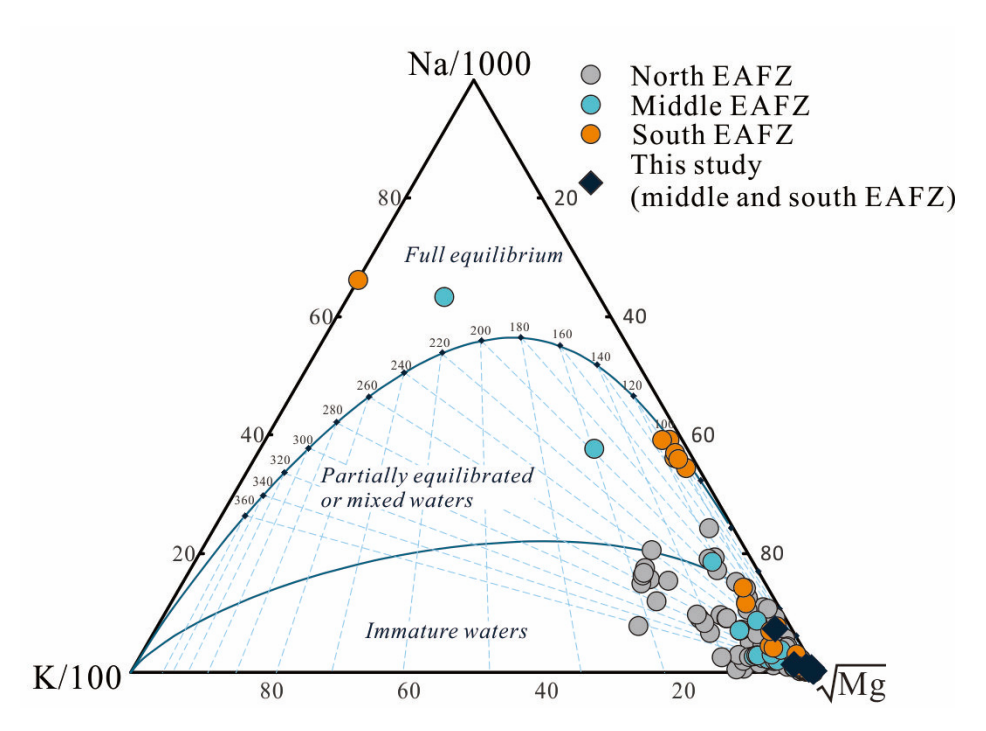


Fig. 4. Na-K-Mg ternary diagram of groundwaters in EAFZ. Literature data source is consistent with Fig. 2.

5.1.3 87Sr/86Sr characteristics of groundwaters

Radiogenic strontium isotopes (87Sr/86Sr) serve as robust tracers of groundwater provenance. The measured 87Sr/86Sr ratios (0.7053–0.713) across EAFZ groundwaters reflect multi-source mixing processes. Central-southern groundwaters integrate signatures from: Shallow aquifers: Inheriting Sr from local lithologies (ophiolites) (Oyan, 2018); Modern seawater: 87Sr/86Sr = 0.7092–0.7096 (Mediterranean seawater) (Banner, 2004; Bernat et al., 1972); River inputs: Enriched ratios (>0.710) from silicate weathering. Binary mixing models using 87Sr/86Sr vs. Ca/Sr ratios (Fig. 5) quantify source contributions: Carbonate weathering dominates, consistent with Ca-HCO₃ hydrochemical type; Ophiolite contributions <10% (except Mg²+-rich samples near ultramafic outcrops); Evaporite dissolution contributes 0–20% (≤50% in localized high-SO₄²- zones). Sr isotope framework corroborates earlier findings of shallow-dominated circulation in central-southern EAFZ.

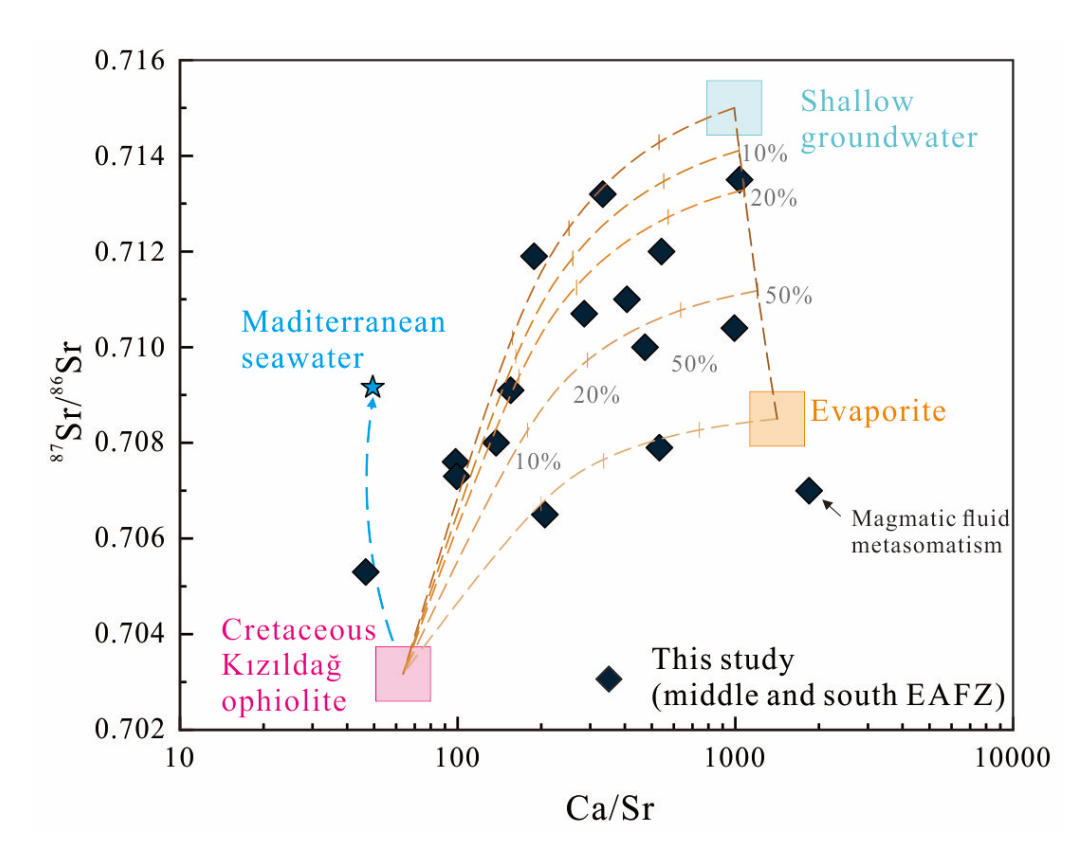


Fig. 5. 87 Sr/ 86 Sr vs. Ca/Sr of groundwaters in the EAFZ. The mixing-boundary lines are built with the following end members: Mediterranean Sea water Ca = 411ppm, Sr = 8.30ppm 87 Sr/ 86 Sr = 0.7092 (Banner, 2004; Bernat et al., 1972); Cretaceous Kızıldağ ophiolite CaO = 9.7%, Sr = 1088.10ppm 87 Sr/ 86 Sr = 0.7032 (Oyan, 2018); Shallow groundwater (HS08) Ca = 55.34ppm, Sr = 0.06ppm 87 Sr/ 86 Sr = 0.7150 (Affected by silicate weathering); Evaporite CaO = 29.5%, Sr = 149ppm 87 Sr/ 86 Sr = 0.7085 (Güngör Yeşilova and Baran, 2023).

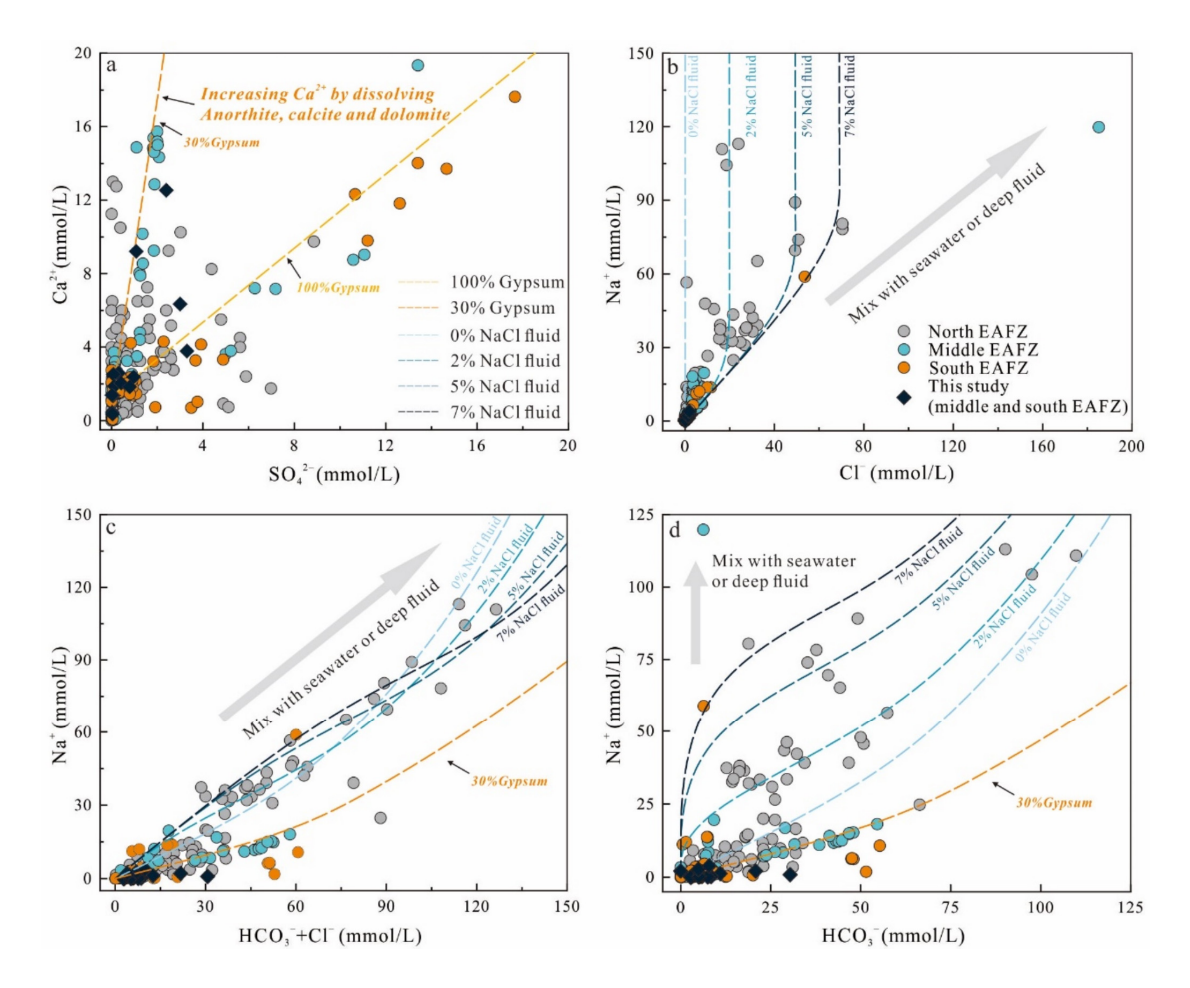


Fig. 6. Characteristics of chemical components of groundwaters in the EAFZ, during water-rock interaction. The dashed line is the numerical simulation result of PHREEQC. a: Ca²⁺ vs SO₄²⁻, b: Na⁺ vs Cl⁻, c: Na⁺ vs HCO₃⁻+Cl⁻ and d: Na⁺ vs HCO₃⁻. The simulation calculations are detailed in Supporting Information Part 1. Literature data source is consistent with Fig. 2.

5.2 The groundwater circulation in different segments of EAFZ

5.2.1 Water-rocks interaction

Pre-seismic whitish discoloration and turbidity anomalies observed at spring HS04 and well HS14 monitoring stations likely reflect seismically induced perturbations to water-rock equilibrium (Video 1 and 2). To validate this hypothesis, we conducted numerical simulations of water-rock interaction processes across distinct segments of EAFZ, aiming to reconstruct their hydrochemical evolution.

Fig. 6 indicates pronounced disparities in groundwater chemistry between northern and central-southern segments. As discussed, elevated Na⁺ and Cl⁻ concentrations in northern groundwaters suggest magmatic fluid contributions. During ascent, these deep-sourced Na-Cl rich fluids mix with shallow groundwater while reacting with surrounding rocks. To quantify magmatic mixing ratios and reaction pathways, we first characterized dominant lithologies in the northern EAFZ—basalt, basaltic andesite, and sedimentary

cover (clastics and carbonates). CIPW norm calculations were employed to estimate mineral abundances, followed by PHREEQC-based reactive transport modeling (Parkhurst and Appelo, 2013) (see Supplementary File 1 for parameters). Simulation results (Fig. 6) demonstrate that linear correlations between Na⁺ and (HCO₃⁻⁺ Cl⁻) arise from magmatic NaCl fluid-carbonate interactions, with magmatic contributions accounting for 0–7% of total mixing.

In contrast, central–southern groundwaters lack magmatic signatures but exhibit Ca²⁺–SO₄²⁻ covariation indicative of anhydrite dissolution (Fig. 6). Central segment waters reflect mixed carbonate- anhydrite controls (30% anhydrite contribution), while southern systems are dominated by anhydrite-derived solutes (100%), sourced from extensive evaporite deposits of the paleo–Amik Lake. Silica–enthalpy mixing models estimate reservoir temperatures of 234°C (HS04) and 155°C (HS14) (Fig. 7a), under which anhydrite saturation indices confirm its dissolution dominance (Fig. 7b). Notably, HS14—located 20 km from the paleo–Amik Basin—displayed prominent pre-seismic turbidity anomalies, likely triggered by earthquake-driven disruption of anhydrite equilibrium. Coseismic changes in temperature, pressure, fracture density, and circulation depth may have enhanced evaporite dissolution, increasing

groundwater salinity.

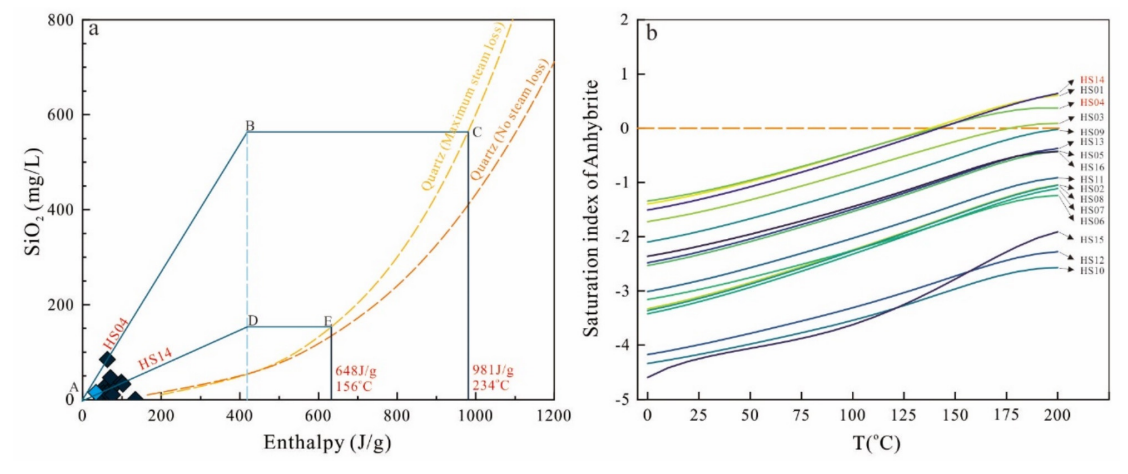


Fig. 7. a: Silica-enthalpy model of groundwaters in EAFZ. b: Temperature versus variation of anhydrite saturation indices of groundwaters in EAFZ. The enthalpies and reservoir temperatures of sample HS04 and HS14 are 981 J/g, 234 °C and 648 J/g, 156 °C respectively. The blue diamond is sample HS08, which is river water. At reservoir temperature, the anhydrite in HS04 and HS14 samples is saturated, indicating that anhydrite dissolution occurs during the water-rock reaction.

5.2.2 Contribution of mantle degassing to EAFZ groundwater circulation

Geochemical studies of EAFZ geothermal gases indicate significant mantle degassing (Fig. 8), where sulfur volatiles (e.g., SO₂ and H₂S) ascend through fault conduits and oxidize upon mixing with shallow

groundwater, ultimately mobilizing as $SO_4^{2^-}$ in thermal fluids. Consequently, mantle-derived sulfur contributions to groundwater sulfate inventories cannot be disregarded. Lacking O_2 was detected in EAFZ geothermal gases suggested that the dissolved oxygen may have been consumed (Italiano et al., 2013; Yuce et al., 2014). However, it is important to note that H_2S , H_2 , and CH_4 can all react with oxygen. Thermodynamic calculations indicate that CH_4 is more favorable than H_2S in oxidation reactions (ΔG° $CH_4 = -818.1$ kJ/mol, ΔG° $H_2S = -494.2$ kJ/mol, at 298 K and 1atm). In actual geothermal systems, however, the depletion of H_2S is more commonly observed than the depletion of CH_4 . We propose the following possible explanations: 1) Oxidation of H_2S : While thermodynamic calculations predict CH_4 oxidation first, a small amount of H_2S might still be oxidized simultaneously with CH_4 . Due to the much lower concentration of H_2S in geothermal systems compared to CH_4 , H_2S is consumed more quickly, leaving CH_4 with a higher residual concentration. 2) Exogenous CH_4 Supply: In addition to mantle-derived CH_4 , other sources of CH_4 , such as biogenic CH_4 and thermogenic CH_4 (e.g., serpentinization), may contribute to the geothermal system. These external sources could increase the concentration of CH_4 in the geothermal fluids.

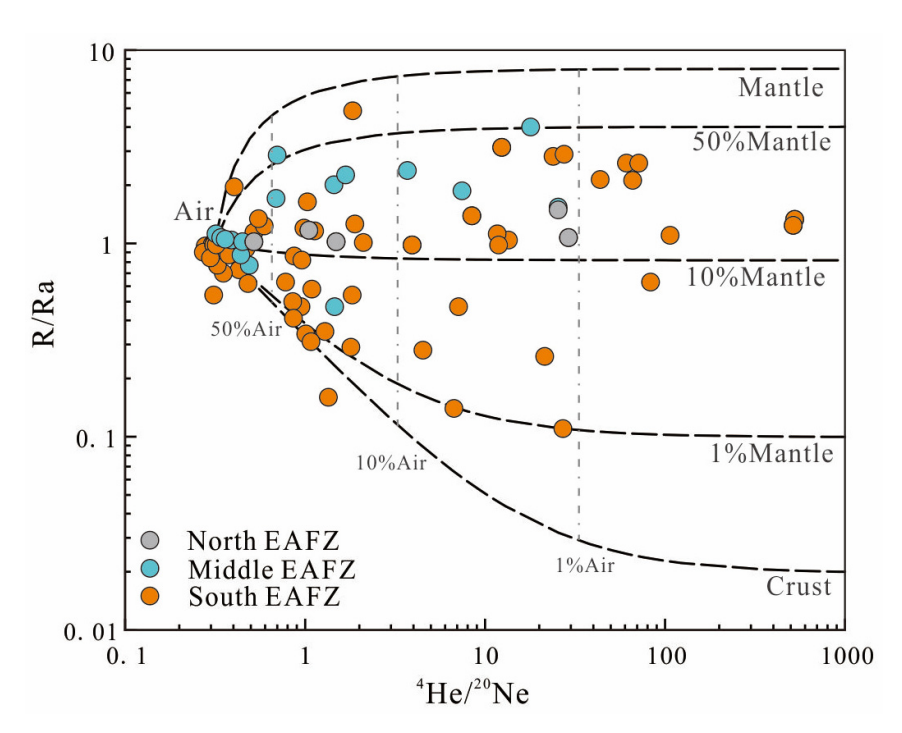


Fig. 8. Helium isotope ratios (R/Ra, Ra = air 3 He/ 4 He = 1.39 × 10-6) versus 4 He/ 2 0Ne ratios for EAFZ gas samples. The mixing-boundary lines are built with the following end members: Air R/Ra = 1 and 4 He/ 2 0Ne = 0.318; mantle R/Ra = 8 and 4 He/ 2 0Ne = 1000; continental crust R/Ra = 0.02 and 4 He/ 2 0Ne = 1000 (Sano and Wakita, 1985). Literature data source from (D'Alessandro et al., 2018; Inguaggiato et al., 2016; Italiano et al., 2013; YASİN and YÜCE, 2023; Yuce et al., 2014; Yuce and Taskiran, 2013).

However, previous studies have shown that the geothermal gas in the southern segment of EAFZ has more crustal source components than northern segment (Fig. 8). Furthermore, isotopic evidence confirms substantial biogenic and serpentinization-derived CH₄ inputs (Italiano et al., 2013; Yan et al., 2024), whereas H₂S remains below detection thresholds. This implies that while H₂S may transiently influence redox cycling, its low abundance limits long-term impacts. Instead, post-seismic SO₄²⁻ surges likely originate from shallow evaporite dissolution (anhydrite) or low-temperature metamorphic anhydrite hydration—processes amplified by coseismic fracture propagation and fluid remobilization.

5.3 Geothermal fluid circulation model in the EAFZ

327

328

329

330

331

332

333

334

335

336

337

338

339

340

341

342

343

344

345

346

347

348

349

350

351

352

353

354

355

As discussed above, EAFZ's geothermal fluid circulation model is shown in the Fig. 9. Beginning in the Late Cretaceous, as the New Tethys Ocean closed, Arabia-Eurasia collision zone have accommodated ~350 km of convergence, making crust up to 45 km thick, and causing >2 km of uplift (Yönlü et al., 2017). Arabian lithospheric mantle extends 50~150 km north beneath Anatolian crust (Whitney et al., 2023). Subsequently, the "roll back" and "slab break" occurred, resulting in extensive volcanic and devastating earthquakes, including those of February 6, 2023 in East Anatolian Plateau (Zhou et al., 2024). The collision of the Eurasian and Arabian plates caused Anatolian microplate was extruding westwards, which lead to EAFZ at a high strike-slip rate of ~11 mm/yr (Pousse - Beltran et al., 2020), and accompanied by counterclockwise rotation with a rotation rate of 1.053 ±0.015°/Ma (Simão et al., 2016). In this tectonic context, EAFZ remains active for a long time. Paleoseismic studies have shown that EAFZ has had many large earthquakes in its history (Carena et al., 2023; Hubert-Ferrari et al., 2020; Sparacino et al., 2022; Tan et al., 2008; Yönlü et al., 2017), with the largest magnitude reaching Mw 8.2 (Carena et al., 2023). Fault that cut through the crust provide channels for material and energy to rise up from mantle, which makes EAFZ geothermal gas contain a high proportion of mantle-derived compositions (Aydin et al., 2020; Italiano et al., 2013; Yuce et al., 2014). However, the transport of geothermal gas and geothermal water appears to be decoupled. On the one hand, deep geothermal fluid stays deep under the influence of gravity and less diffusive, compare to geothermal gas. On the other hand, the geothermal fluid was diluted due to the infiltration of a large amount of shallow cold water after the double earthquakes in February 2023 (Mw 7.8 and Mw 7.6). Our interpretation can better explain the lack of deep fluid signal in the groundwater studied in this study. Subsequently, at a depth of 4km, gas-water interaction process was experienced. Finally rose to the

surface and discharged into the atmosphere. On the contrary, the circulating groundwater has undergone complex water-rock interaction processes such as anhydrite, calcite, dolomite, anorthite and serpentinization (Fig. 9).

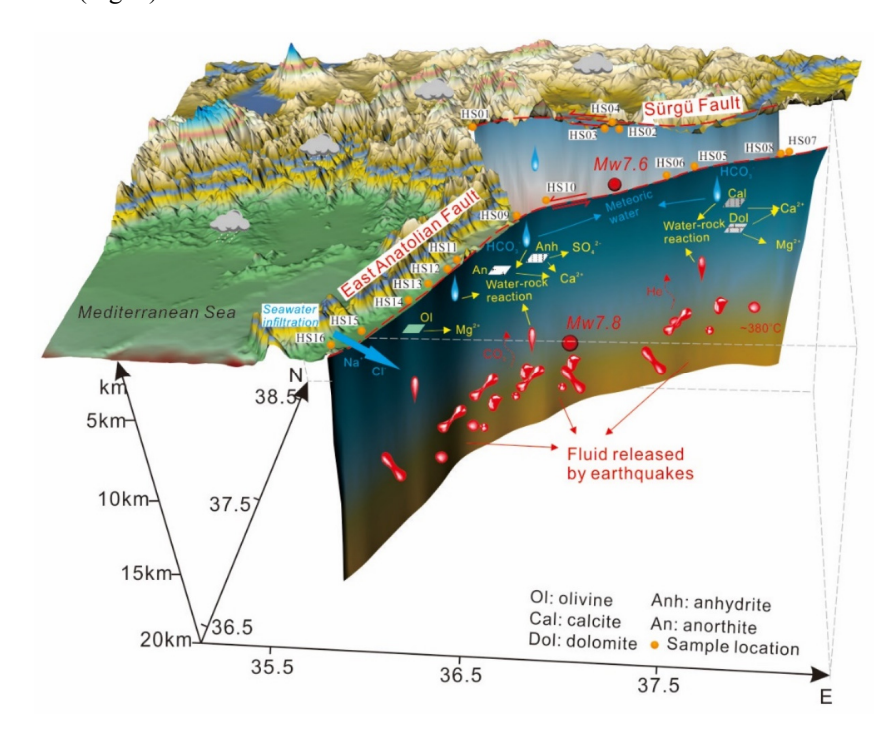


Fig. 9. The genesis model of the geothermal fluids in the EAFZ. The deep geothermal fluid was diluted due to the infiltration of a large amount of shallow cold water. In the shallow crust, gas-water interaction process and water-rock interaction processes were experienced. The gases rose to the surface and discharged into the atmosphere. The circulating groundwater has undergone complex such as anhydrite, calcite, dolomite, anorthite and serpentinization.

5.4 The relationship between geothermal fluid and earthquake forecasting

Earthquake forecasting is a grand goal pursued by human beings, but also one of the most difficult goals. Various physical, chemical and biological techniques are used for earthquake forecasting (Bayrak et al., 2015; Bürgmann, 2023; Güleç et al., 2002; Jordan et al., 2011; Kwiatek et al., 2023; Luo et al., 2024; Luo et al., 2023; Miller et al., 2004; Nalbant et al., 2002; Skelton et al., 2014; Tsunogai and Wakita, 1995; Wakita et al., 1980). As a link between the shallow (crust) and the deep (mantle), geothermal fluids can react to various diseases just like human blood. In earlier studies, researchers found that the anomaly of chemical indicators in geothermal fluids could be used for earthquake forecasting e.g., (Güleç et al., 2002; King et al., 2006; Miller et al., 2004; Perez et al., 2008; Poitrasson et al., 1999; Tsunogai and Wakita, 1995), but due to limited technology and funding, such research requiring long-term and large-scale monitoring is difficult to carry out (Ingebritsen and Manga, 2014). With the advancement of

technology, more and more automated equipment and the development of 5G communication technology
make long-term automatic monitoring possible, e.g., (Barbieri et al., 2021; Boschetti et al., 2022;
Franchini et al., 2021; Liang et al., 2023; Luo et al., 2024; Luo et al., 2023; Skelton et al., 2014; Wang
et al., 2023a). However, before geothermal fluid is really used in earthquake prediction, there is a problem
that must be solved (i.e. to understand the relationship between geothermal fluid and earthquake). Its
essence is to restore the origin and evolution process of geothermal fluid (Boschetti et al., 2022).
For a long time, researchers have been searching for the information of the deep fluid in the fault zone,
trying to link the earthquake with the deep fluid activity (Liang et al., 2023; Luo et al., 2023; Yan et al.,
2024). However, deep information is easily changed during upward migration, and sometimes even lacks
deep information, just like the EAFZ groundwater in this study (Fig. 6). This seems to limit the ability
of groundwater to be used for earthquake prediction. In fact, chemical anomalies related to seismic
activity can still be found in some shallow circulating groundwater (e.g., SO_4^{2-}) (Luo et al., 2023).
Moreover, the shallower water-rock interactions are more sensitive to the environment. Shallow-
circulation water-rock interactions are fundamentally controlled by host rock lithology, where distinct
lithologic units impart unique hydrochemical signatures to circulating fluids—enabling specific strata to
function as target indicator horizons for tracing seismotectonic hazards. Groundwater-rock systems
typically maintain equilibrium under stable conditions, but external perturbations (e.g., seismic stress or
rainfall variability) can disrupt regional hydrogeochemical equilibria, accelerate dissolution of target
horizons like evaporites, and amplify water-rock interaction intensity, thereby generating diagnostic
solute anomalies. For instance, anhydrite dissolution manifests as covariant Ca ²⁺ -SO ₄ ²⁻ anomalies;
accelerated dissolution from seismic/seasonal forces triggers synchronous Ca-SO ₄ ²⁻ concentration spikes
and salinity increases, producing macroscopic turbidity or whitening. Consequently, analyzing regional
hydrogeochemical baselines to identify aquifer-specific target horizons, implementing their continuous
monitoring, and establishing localized evaluation thresholds enables early warning systems for
geohazard precursors.
Anhydrite are widely distributed in nature, and its formation is related to evaporite or hydrothermal
metasomatism. Dissolution and precipitation of anhydrite are often observed in groundwater. Its
solubility is greatly affected by environmental conditions (temperature, pH, pressure surrounding rock
condition etc.) and they are potential indicators of tectonic activity (Jin et al., 2016). After the 2023 Mw
7.8 and 2023 Mw 7.6 earthquake, in the absence of deep fluid signals, we observed anhydrite dissolution 19

6). Similar SO₄²⁻ anomalies have also been found in the eastern Tibetan Plateau (Li et al., 2021; Luo et al., 2023) and southeast China (Wang et al., 2021). Therefore, we suggest that anhydrite can be used as a potential tectonic activity index. However, although anhydrite's potential as a tectonic activity proxy is significant, its shallow crustal occurrence renders it susceptible to climatic perturbations (e.g., rainfall, evaporation). As evidenced in Fig. 6, post-seismic SO₄²⁻ and Ca²⁺ concentrations show no statistically significant deviations from background levels during quiescent periods, underscoring the challenge of filtering out climatic noise. While statistical correlations tentatively position anhydrite dissolution as a fault activity indicator, advancing this paradigm requires: Long-term, high-resolution monitoring to disentangle tectonic vs. meteoric signals (e.g., Thermal-hydrothermal experimental and statistical or machine learning approaches (e.g., PCA, random forests)); Mechanistic models integrating fracture permeability dynamics with anhydrite solubility kinetics. This study's key contribution lies in establishing fault-driven permeability changes as a viable driver of anhydrite dissolution. We propose a novel conceptual framework for fault activity monitoring via groundwater systems—one that prioritizes reactive minerals in shallow water-rock interactions over traditional deep fluid signals.

at central-southern segments of EAFZ, which are likely to have been affected by seismic activity (Fig.

6 Conclusions

406

407

408

409

410

411

412

413

414

415

416

417

418

419

420

421

422

423

424

425

- Segmented groundwater provenance: Northern groundwaters represent mixing between mantle-derived magmatic fluids (0–7%) and shallow meteoric waters, while central-southern systems are dominated by carbonate-evaporite weathering with localized seawater/halite inputs.
- Tectono-Climatic controls on water-rock interactions: Plagioclase-carbonate dissolution dominates northern segments, whereas anhydrite dissolution (30–100%) in central-southern segments correlates
- 429 with fault permeability changes. Seismically enhanced fracture networks amplify evaporite dissolution,
- 430 driving hydrochemical anomalies.
- 431 Anhydrite as a tectonic activity tracer: Despite climatic noise, anhydrite dissolution kinetics exhibit
- 432 stress-state sensitivity. Their ubiquity and rapid stress response position anhydrite as a potential tracer
- 433 for real-time fault activity monitoring.

The fundamental contribution of this study lies in proposing a novel research paradigm: identifying suitable target indicator horizons. Regionally variable minerals may serve as diagnostic tracers. By analyzing the regional hydrogeochemical context to elucidate groundwater circulation and water-rock interaction mechanisms, we can identify optimal target horizons for specific areas, implement continuous monitoring, establish region-specific evaluation metrics, thus achieving early warning capabilities for seismically induced geohazards.

- 440 Code and data availability. All water data are listed in the text or in the Supporting Information.
- **Supplement.** See Supporting Information.
- 442 Authorship contributions. Zebin Luo: Conceptualization, Methodology, Software, Writing-Original
- 443 Draft, Writing-Review and Editing. Xiaocheng Zhou: Conceptualization, Validation. Yueren Xu:
- 444 Investigation. Peng Liang: Investigation. Huiping Zhang: Investigation. Jinlong Liang: Validation.
- 445 Zhaojun Zeng: Investigation. Yucong Yan: Investigation. Zheng Gong: Investigation. Shiguang Wang:
- 446 Investigation. Chuanyou Li: Investigation. Zhikun Ren: Investigation. Jingxing Yu: Investigation.
- **Zifa Ma:** Investigation. **Junjie Li:** Investigation.
- 448 Competing Interests. The authors declare that they have no known competing financial interests or
- personal relationships that could have appeared to influence the work reported in this paper.
- 450 **Acknowledgements.** We would like to thank the Associate Editor Prof. Heng Dai, Walter D'Alessandro
- 451 Giovanni Martinelli, Hafidha Khebizi and another anonymous reviewers for their constructive comments,
- suggestions and corrections. We also thank Dr. Yinchun Wang Dr. Renjie Li and Dr. Yi Yu for discussion,
- 453 Dr. Shiqi Zhang for her help for diagram drawing.
- 454 Financial support. The work was funded by National Key Research and Development Project
- 455 (2024ZD1000503, 2023YFC3012005-1), Central Public-interest Scientific Institution Basal Research
- Fund (CEAIEF20240405, CEAIEF2022030200, CEAIEF2022030205), the National Natural Science
- 457 Foundation of China (41673106, 4193000170), IGCP Project 724.

458 References

- Aydin, H., Karakuş, H., and Mutlu, H.: Hydrogeochemistry of geothermal waters in
- 460 eastern Turkey: Geochemical and isotopic constraints on water-rock interaction,
- Journal of Volcanology and Geothermal Research, 390, 2020.
- Baba, A., Şaroğlu, F., Akkuş, I., Özel, N., Yeşilnacar, M. İ., Nalbantçılar, M. T., Demir,
- 463 M. M., Gökçen, G., Arslan, Ş., Dursun, N., Uzelli, T., and Yazdani, H.: Geological and
- 464 hydrogeochemical properties of geothermal systems in the southeastern region of
- 465 Turkey, Geothermics, 78, 255-271, 2019.
- Banner, J. L.: Radiogenic isotopes: systematics and applications to earth surface
- processes and chemical stratigraphy, Earth-Science Reviews, 65, 141-194, 2004.
- Barbieri, M., Franchini, S., Barberio, M. D., Billi, A., Boschetti, T., Giansante, L., Gori,
- 469 F., Jonsson, S., Petitta, M., Skelton, A., and Stockmann, G.: Changes in groundwater
- 470 trace element concentrations before seismic and volcanic activities in Iceland during
- 471 2010-2018, Science of the Total Environment, 793, 2021.
- Bayrak, E., Yılmaz, Ş., Softa, M., Türker, T., and Bayrak, Y.: Earthquake hazard
- analysis for East Anatolian Fault Zone, Turkey, Natural Hazards, 76, 1063-1077, 2015.
- Bernat, M., Church, T., and Allegre, C. J.: Barium and strontium concentrations in
- Pacific and Mediterranean sea water profiles by direct isotope dilution mass
- spectrometry, Earth and Planetary Science Letters, 16, 75-80, 1972.
- Bilim, F., Aydemir, A., Kosaroglu, S., and Bektas, O.: Effects of the Karacadag Volcanic
- 478 Complex on the thermal structure and geothermal potential of southeast Anatolia,
- Bulletin of Volcanology, 80, 2018.
- Boschetti, T., Barbieri, M., Barberio, M. D., Skelton, A., Stockmann, G., and Toscani,
- 481 L.: Geothermometry and water-rock interaction modelling at Hafralkur: Possible
- 482 implications of temperature and CO2 on hydrogeochemical changes previously linked
- to earthquakes in northern Iceland, Geothermics, 105, 2022.
- Bürgmann, R.: Reliable earthquake precursors?, Science, 381, 266-267, 2023.
- Carena, S., Friedrich, A. M., Verdecchia, A., Kahle, B., Rieger, S., and Kübler, S.:
- 486 Identification of Source Faults of Large Earthquakes in the Turkey Syria Border
- Region Between 1000 CE and the Present, and Their Relevance for the 2023 Mw 7.8
- 488 Pazarcık Earthquake, Tectonics, 42, 2023.
- 489 Craig, H.: Isotopic Variations in Meteoric Waters, Science, 133, 1702-1703, 1961.
- 490 D'Alessandro, W., Yüce, G., Italiano, F., Bellomo, S., Gülbay, A. H., Yasin, D. U., and
- 491 Gagliano, A. L.: Large compositional differences in the gases released from the
- 492 Kizildag ophiolitic body (Turkey): Evidences of prevailingly abiogenic origin, Marine
- and Petroleum Geology, 89, 174-184, 2018.
- 494 Franchini, S., Agostini, S., Barberio, M. D., Barbieri, M., Billi, A., Boschetti, T., Pennisi,
- 495 M., and Petitta, M.: HydroQuakes, central Apennines, Italy: Towards a
- 496 hydrogeochemical monitoring network for seismic precursors and the hydro-seismo-
- sensitivity of boron, Journal of Hydrology, 598, 2021.
- 498 Giggenbach, W. F.: Isotopic shifts in waters from geothermal and volcanic systems
- along convergent plate boundaries and their origin, Earth and Planetary Science Letters,
- 500 113, 495-510, 1992.

- 501 Güleç, N. and Hilton, D. R.: Turkish geothermal fields as natural analogues of CO 2
- storage sites: Gas geochemistry and implications for CO 2 trapping mechanisms,
- 503 Geothermics, 64, 96-110, 2016.
- 504 Güleç, N., Hilton, D. R., and Mutlu, H.: Helium isotope variations in Turkey::
- relationship to tectonics, volcanism and recent seismic activities, Chemical Geology,
- 506 187, 129-142, 2002.
- 507 Güngör Yeşilova, P. and Baran, O.: Origin and Paleoenvironmental Conditions of the
- 508 Köprüağzı Evaporites (Eastern Anatolia, Turkey): Sedimentological, Mineralogical and
- Geochemical Constraints, Minerals, 13, 282, 2023.
- Hubert-Ferrari, A., Lamair, L., Hage, S., Schmidt, S., Çağatay, M. N., and Avşar, U.: A
- 3800 yr paleoseismic record (Lake Hazar sediments, eastern Turkey): Implications for
- the East Anatolian Fault seismic cycle, Earth and Planetary Science Letters, 538, 2020.
- Ingebritsen, S. E. and Manga, M.: EARTHQUAKES Hydrogeochemical precursors,
- 514 Nature Geoscience, 7, 697-698, 2014.
- 515 Inguaggiato, C., Censi, P., D'Alessandro, W., and Zuddas, P.: Geochemical
- characterisation of gases along the dead sea rift: Evidences of mantle-co2 degassing,
- Journal of Volcanology and Geothermal Research, 320, 50-57, 2016.
- 518 Italiano, F., Sasmaz, A., Yuce, G., and Okan, O. O.: Thermal fluids along the East
- Anatolian Fault Zone (EAFZ): Geochemical features and relationships with the tectonic
- setting, Chemical Geology, 339, 103-114, 2013.
- 521 Jin, Z., West, A. J., Zhang, F., An, Z., Hilton, R. G., Yu, J., Wang, J., Li, G., Deng, L.,
- and Wang, X.: Seismically enhanced solute fluxes in the Yangtze River headwaters
- following the AD 2008 Wenchuan earthquake, Geology, 44, 47-50, 2016.
- Jordan, T. H., Chen, Y.-T., Gasparini, P., Madariaga, R., Main, I., Marzocchi, W.,
- Papadopoulos, G., Sobolev, G., Yamaoka, K., and Zschau, J.: Operational Earthquake
- Forecasting: State of Knowledge and Guidelines for Utilization, Annals of Geophysics,
- 527 54, 315-391, 2011.
- Karaoğlu, Ö., Bazargan, M., Baba, A., and Browning, J.: Thermal fluid circulation
- 529 around the Karliova triple junction: Geochemical features and volcano-tectonic
- implications (Eastern Turkey), Geothermics, 81, 168-184, 2019.
- Karaoğlu, Ö., Browning, J., Salah, M. K., Elshaafi, A., and Gudmundsson, A.: Depths
- of magma chambers at three volcanic provinces in the Karlıova region of Eastern
- Turkey, Bulletin of Volcanology, 80, 2018.
- Karaoğlu, Ö., Gülmez, F., Göçmengil, G., Lustrino, M., Di Giuseppe, P., Manetti, P.,
- 535 Savaşçın, M. Y., and Agostini, S.: Petrological evolution of Karlıova-Varto volcanism
- 536 (Eastern Turkey): Magma genesis in a transtensional triple-junction tectonic setting,
- 537 Lithos, 364-365, 2020.
- King, C.-Y., Zhang, W., and Zhang, Z.: Earthquake-induced Groundwater and Gas
- Changes, Pure and Applied Geophysics, 163, 633-645, 2006.
- Kwiatek, G., Martinez-Garzon, P., Becker, D., Dresen, G., Cotton, F., Beroza, G. C.,
- Acarel, D., Ergintav, S., and Bohnhoff, M.: Months-long seismicity transients preceding
- the 2023 M(W) 7.8 Kahramanmaras earthquake, Turkiye, Nat Commun, 14, 7534, 2023.
- Lanari, R., Boutoux, A., Faccenna, C., Herman, F., Willett, S. D., and Ballato, P.:
- 544 Cenozoic exhumation in the Mediterranean and the Middle East, Earth-Science

- 545 Reviews, 237, 2023.
- Li, C., Zhou, X., Yan, Y., Ouyang, S., and Liu, F.: Hydrogeochemical Characteristics of
- 547 Hot Springs and Their Short-Term Seismic Precursor Anomalies along the Xiaojiang
- Fault Zone, Southeast Tibet Plateau, Water, 13, 2021.
- 549 Liang, J., Yu, Y., Shi, Z., Li, Z., Huang, Y., Song, H., Xu, J., Wang, X., Zhou, X., Huang,
- 550 L., Luo, Z., Tong, J., and Zhai, W.: Geothermal springs with high δ13CCO2-DIC along
- 551 the Xianshuihe fault, Western Sichuan, China: A geochemical signature of enhanced
- deep tectonic activity, Journal of Hydrology, 623, 129760, 2023.
- 553 Liang, P., Xu, Y., Zhou, X., Li, Y., Tian, Q., Zhang, H., Ren, Z., Yu, J., Li, C., Gong, Z.,
- Wang, S., Dou, A., Ma, Z., and Li, J.: Coseismic surface ruptures of MW7.8 and MW7.5
- earthquakes occurred on February 6, 2023, and seismic hazard assessment of the East
- Anatolian Fault Zone, Southeastern Türkiye, Science China Earth Sciences, 68, 611-
- 557 625, 2024.
- Liu, X., Dong, S., Yue, Y., Guan, Q., Sun, Y., Chen, S., Zhang, J., and Yang, Y.:
- 87Sr/86Sr isotope ratios in rocks determined using inductively coupled plasma tandem
- mass spectrometry in O2 mode without prior Sr purification, Rapid Communications
- in Mass Spectrometry, 34, e8690, 2020.
- 562 Luo, Z., Yang, M., Zhou, X., Liu, G., Liang, J., Liu, Z., Hua, P., Ma, J., Hu, L., Sun, X.,
- 563 Cui, B., Wang, Z., and Chen, Y.: Evaluation of Various Forms of Geothermal Energy
- Release in the Beijing Region, China, Water, 16, 2024.
- 565 Luo, Z., Zhou, X., He, M., Liang, J., Li, J., Dong, J., Tian, J., Yan, Y., Li, Y., Liu, F.,
- Ouyang, S., Liu, K., Yao, B., Wang, Y., and Zeng, Z.: Earthquakes evoked by lower
- 567 crustal flow: Evidence from hot spring geochemistry in Lijiang-Xiaojinhe fault, Journal
- of Hydrology, 619, 129334, 2023.
- 569 Ma, Z., Li, C., Jiang, Y., Chen, Y., Yin, X., Aoki, Y., Yun, S. H., and Wei, S.: Space
- 570 Geodetic Insights to the Dramatic Stress Rotation Induced by the February 2023
- 571 Turkey Syria Earthquake Doublet, Geophysical Research Letters, 51, 2024.
- Maden, N. and Öztürk, S.: Seismic b-Values, Bouguer Gravity and Heat Flow Data
- Beneath Eastern Anatolia, Turkey: Tectonic Implications, Surveys in Geophysics, 36,
- 574 549-570, 2015.
- 575 Miller, S. A., Collettini, C., Chiaraluce, L., Cocco, M., Barchi, M., and Kaus, B.:
- Aftershocks driven by a high-pressure CO2 source at depth, Nature, 427, 724-727, 2004.
- Nalbant, S. S., McCloskey, J., Steacy, S., and Barka, A. A.: Stress accumulation and
- increased seismic risk in eastern Turkey, Earth and Planetary Science Letters, 195, 291-
- 579 298, 2002.
- Okan, O. O., Kalender, L., and Cetindag, B.: Trace-element hydrogeochemistry of
- thermal waters of Karakocan (Elazig) and Mazgirt (Tunceli), Eastern Anatolia, Turkey,
- Journal of Geochemical Exploration, 194, 29-43, 2018.
- Över, S., Demirci, A., and Özden, S.: Tectonic implications of the February 2023
- Earthquakes (Mw7.7, 7.6 and 6.3) in south-eastern Türkiye, Tectonophysics, 866, 2023.
- Oyan, V.: Petrogenesis of the Quaternary mafic alkaline volcanism along the African-
- Anatolian plates boundary in Turunçlu-Delihalil (Osmaniye) region in southern Turkey,
- 587 Lithos, 314-315, 630-645, 2018.
- Özkan, A., Solak, H. İ., Tiryakioğlu, İ., Şentürk, M. D., Aktuğ, B., Gezgin, C., Poyraz,

- 589 F., Duman, H., Masson, F., Uslular, G., Yiğit, C. Ö., and Yavaşoğlu, H. H.:
- 590 Characterization of the co-seismic pattern and slip distribution of the February 06, 2023,
- Kahramanmaraş (Turkey) earthquakes (Mw 7.7 and Mw 7.6) with a dense GNSS
- network, Tectonophysics, 866, 2023.
- Pan, S., Kong, Y., Wang, K., Ren, Y., Pang, Z., Zhang, C., Wen, D., Zhang, L., Feng,
- 594 Q., Zhu, G., and Wang, J.: Magmatic origin of geothermal fluids constrained by
- 595 geochemical evidence: Implications for the heat source in the northeastern Tibetan
- Plateau, Journal of Hydrology, 603, 2021.
- Parkhurst, D. L. and Appelo, C. A. J.: Description of input and examples for PHREEQC
- version 3: a computer program for speciation, batch-reaction, one-dimensional
- transport, and inverse geochemical calculations, U.S. Geological Survey, Reston, VA,
- 600 2013.
- Pasvanoglu, S.: Geochemistry and conceptual model of thermal waters from Ercis -
- Zilan Valley, Eastern Turkey, Geothermics, 86, 2020.
- Perez, N. M., Hernandez, P. A., Igarashi, G., Trujillo, I., Nakai, S., Sumino, H., and
- Wakita, H.: Searching and detecting earthquake geochemical precursors in CO2-rich
- groundwaters from Galicia, Spain, Geochemical Journal, 42, 75-83, 2008.
- Poitrasson, F., Dundas, S. H., Toutain, J.-P., Munoz, M., and Rigo, A.: Earthquake-
- related elemental and isotopic lead anomaly in a springwater, Earth and Planetary
- 608 Science Letters, 169, 269-276, 1999.
- Pousse Beltran, L., Nissen, E., Bergman, E. A., Cambaz, M. D., Gaudreau, É.,
- Karasözen, E., and Tan, F.: The 2020 Mw 6.8 Elazığ (Turkey) Earthquake Reveals
- Rupture Behavior of the East Anatolian Fault, Geophysical Research Letters, 47, 2020.
- Sano, Y. and Wakita, H.: Geographical distribution of 3He/4He ratios in Japan:
- 613 Implications for arc tectonics and incipient magmatism, Journal of Geophysical
- Research: Solid Earth, 90, 8729-8741, 1985.
- 615 Simão, N. M., Nalbant, S. S., Sunbul, F., and Komec Mutlu, A.: Central and eastern
- Anatolian crustal deformation rate and velocity fields derived from GPS and earthquake
- data, Earth and Planetary Science Letters, 433, 89-98, 2016.
- 618 Skelton, A., Andren, M., Kristmannsdottir, H., Stockmann, G., Morth, C.-M.,
- 619 Sveinbjoernsdottir, A., Jonsson, S., Sturkell, E., Gudorunardottir, H. R., Hjartarson, H.,
- 620 Siegmund, H., and Kockum, I.: Changes in groundwater chemistry before two
- consecutive earthquakes in Iceland, Nature Geoscience, 7, 752-756, 2014.
- 622 Sparacino, F., Galuzzi, B. G., Palano, M., Segou, M., and Chiarabba, C.: Seismic
- 623 coupling for the Aegean Anatolian region, Earth-Science Reviews, 228, 2022.
- Tan, O., Tapirdamaz, M. C., and Yoruk, A.: The earthquake catalogues for Turkey,
- Turkish Journal of Earth Sciences, 17, 405-418, 2008.
- Tsunogai, U. and Wakita, H.: Precursory chemical changes in ground water: kobe
- 627 earthquake, Japan, Science (New York, N.Y.), 269, 61-63, 1995.
- van Hinsbergen, D. J. J., Gürer, D., Koç, A., and Lom, N.: Shortening and extrusion in
- 629 the East Anatolian Plateau: How was Neogene Arabia-Eurasia convergence tectonically
- accommodated?, Earth and Planetary Science Letters, 641, 2024.
- Wakita, H., Nakamura, Y., Kita, I., Fujii, N., and Notsu, K.: Hydrogen release: new
- indicator of fault activity, Science (New York, N.Y.), 210, 188-190, 1980.

- Wang, B., Zhou, X., Zhou, Y., Yan, Y., Li, Y., Ouyang, S., Liu, F., and Zhong, J.:
- 634 Hydrogeochemistry and Precursory Anomalies in Thermal Springs of Fujian
- 635 (Southeastern China) Associated with Earthquakes in the Taiwan Strait, Water, 13, 2021.
- 636 Wang, Y., Zhou, X., Tian, J., Zhou, J., He, M., Li, J., Dong, J., Yan, Y., Liu, F., Yao, B.,
- Wang, Y., Zeng, Z., Liu, K., Li, L., Li, Z., and Xing, L.: Volatile characteristics and
- 638 fluxes of He-CO2 systematics in the southeastern Tibetan Plateau: Constraints on
- regional seismic activities, Journal of Hydrology, 617, 2023a.
- Wang, Z., Zhang, W., Taymaz, T., He, Z., Xu, T., and Zhang, Z.: Dynamic Rupture
- Process of the 2023 Mw 7.8 Kahramanmaraş Earthquake (SE Türkiye): Variable
- Rupture Speed and Implications for Seismic Hazard, Geophysical Research Letters, 50,
- 643 2023b.
- Whitney, D. L., Delph, J. R., Thomson, S. N., Beck, S. L., Brocard, G. Y., Cosca, M.
- A., Darin, M. H., Kaymakci, N., Meijers, M. J. M., Okay, A. I., Rojay, B., Teyssier, C.,
- and Umhoefer, P. J.: Breaking plates: Creation of the East Anatolian fault, the Anatolian
- plate, and a tectonic escape system, Geology, 51, 673-677, 2023.
- 648 Yan, Y., Zhang, Z., Zhou, X., Wang, G., He, M., Tian, J., Dong, J., Li, J., Bai, Y., Zeng,
- 649 Z., Wang, Y., Yao, B., Xing, G., Cui, S., and Shi, Z.: Geochemical characteristics of hot
- springs in active fault zones within the northern Sichuan-Yunnan block: Geochemical
- evidence for tectonic activity, Journal of Hydrology, 635, 2024.
- YASİN, D. and YÜCE, G.: Isotope and hydrochemical characteristics of thermal waters
- along the active fault zone (Erzin-Hatay/Turkey) and their geothermal potential,
- Turkish Journal of Earth Sciences, 32, 721-739, 2023.
- Yönlü, Ö., Altunel, E., and Karabacak, V.: Geological and geomorphological evidence
- 656 for the southwestern extension of the East Anatolian Fault Zone, Turkey, Earth and
- 657 Planetary Science Letters, 469, 1-14, 2017.
- Yuce, G., Italiano, F., D'Alessandro, W., Yalcin, T. H., Yasin, D. U., Gulbay, A. H.,
- Ozyurt, N. N., Rojay, B., Karabacak, V., Bellomo, S., Brusca, L., Yang, T., Fu, C. C.,
- Lai, C. W., Ozacar, A., and Walia, V.: Origin and interactions of fluids circulating over
- the Amik Basin (Hatay, Turkey) and relationships with the hydrologic, geologic and
- tectonic settings, Chemical Geology, 388, 23-39, 2014.
- Yuce, G. and Taskiran, L.: Isotope and chemical compositions of thermal fluids at
- Tekman Geothermal Area (Eastern Turkey), GEOCHEMICAL JOURNAL, 47, 423-
- 665 435, 2013.

- 666 Zeng, Z., Yang, L., Cui, Y., Zhou, X., He, M., Wang, Y., Yan, Y., Yao, B., Hu, X., Shao,
- 667 W., Li, J., and Fu, H.: Assessment of geothermal waters in Yunnan, China: Distribution,
- quality and driving factors, Geothermics, 130, 103323, 2025.
- Zhou, Z., Thybo, H., Artemieva, I. M., Kusky, T., and Tang, C.-C.: Crustal melting and
- 670 continent uplift by mafic underplating at convergent boundaries, Nature
- 671 Communications, 15, 2024.